Available online at www.sciencedirect.com
ScienceDirect
Journal of Catalysis 253 (2008) 1–10
JOURNAL OF CATALYSIS
www.elsevier.com/locate/jcat

Effect of calcination temperature on CrO_x–Y_2O_3 catalysts for fluorination of 2-chloro-1,1,1-trifluoroethane to 1,1,1,2-tetrafluoroethane

Jun He [a], Guan-Qun Xie [a], Ji-Qing Lu [a], Lin Qian [a], Xue-Liang Zhang [b], Ping Fang [a], Zhi-Ying Pu [a], Meng-Fei Luo [a,*]

[a] *Zhejiang Key Laboratory for Reactive Chemistry on Solid Surfaces, Institute of Physical Chemistry, Zhejiang Normal University, Jinhua 321004, China*
[b] *Zhejiang Qu Hua Fluor-Chemistry Company Limited, Quzhou 324004, China*

Received 14 August 2007; revised 28 September 2007; accepted 5 November 2007

Abstract

A series of CrO_x–Y_2O_3 catalysts were prepared by a deposition–precipitation method and tested for the fluorination of 2-chloro-1,1,1-trifluoroethane (CF_3CH_2Cl) to synthesize 1,1,1,2-tetrafluoroethane (CF_3CH_2F). The highest activity was obtained on a pre-fluorinated catalyst calcined at 400 °C, with 19% of CF_3CH_2Cl conversion at 320 °C. The effect of the calcination temperature on the CrO_x species was investigated. X-ray diffraction and Raman results indicated that the CrO_x species (Cr(VI)) were well dispersed on the catalyst surface when the catalyst was calcined at 400 °C. With increasing calcination temperature, most of the CrO_x species changed from high oxidation state Cr(VI) to low oxidation state Cr(V) or Cr(III) species, which resulted in difficulty in pre-fluorination of the catalyst. It was also found that the CrF_x, CrO_xF_y or $Cr(OH)_xF_y$ phases originated from high oxidation state Cr(VI) species were the active sites for the fluorination reaction.

Keywords: Fluorination; 1,1,1,2-tetrafluoroethane; Cr catalyst; Y_2O_3; Active sites

1. Introduction

Chlorofluorocarbons (CFCs) are considered as stratosphere ozone depletion substances (ODS) [1]. According to the Montreal Protocol, CFCs will be abandoned by 2010 in developing countries and has been forbidden since 2000 in developed countries. As CFCs are widely used in the refrigeration field and their importance in the industry, preparation of hydrofluorocarbon (HFC) alternatives has attracted much attention. For example, 1,1,1,2-tetrafluoroethane (CF_3CH_2F) has been considered as a promising alternative of dichlorodifluoromethane (CF_2Cl_2) for its zero ozone depletion potential (ODP) and low global warming potential (GWP) values.

One of the synthesis routes for CF_3CH_2F is gas-phase fluorination of 2-chloro-1,1,1-trifluoroethane (CF_3CH_2Cl) with HF over CrF_3 and CrO_x catalysts supported on MgF_2, AlF_3, MgO or Al_2O_3 [2–6]. Cho et al. [4] found that Cr/MgO catalyst was the best catalyst for the fluorination of CF_3CH_2Cl and the catalytic activity was greatly affected by the pretreatment conditions. Besides, they have found that the chromium fluoride CrF_x or oxyfluoride CrO_xF_y were the active sites for the reaction while crystalline Cr_2O_3 was an inactive catalyst. In addition, it was found that the CrO_xF_y phase exhibited significantly higher catalytic activity in dismutation of CCl_2F_2 and fluorination of CF_3CH_2Cl than the pure oxide (Cr_2O_3) and fluoride (α-CrF_3 and β-CrF_3) [5,7,8]. Quan et al. [9] found that Cr species with high oxidation state shows higher catalytic activity than Cr(III) in fluorination of CH_2Cl_2 to CH_2F_2. However, more evidence is needed to further understand the active sites, because at present evolution of the active sites such as CrF_x and CrO_xF_y remains unclear. Furthermore, as thermal pretreatment would cause structural change of the Cr catalysts, effect of calcination temperature on the structure of the catalysts and catalytic activity is of great importance.

In this work, yttrium oxide (Y_2O_3) was used as a support for chromium oxide catalysts. The catalytic performance of the CrO_x–Y_2O_3 catalysts was tested for fluorination of CF_3CH_2Cl

* Corresponding author. Fax: +86 579 82282595.
E-mail address: mengfeiluo@zjnu.cn (M.-F. Luo).

0021-9517/$ – see front matter
doi:10.1016/j.jcat.2007.11.005

to CF_3CH_2F. By using various characterization techniques, effect of calcination temperature on the structure and composition of the catalysts was investigated and correlated to the catalytic performance. Also, the evolution of the active sites for this reaction was discussed.

2. Experimental

2.1. Catalyst preparation

The CrO_x–Y_2O_3 catalysts were prepared by a deposition–precipitation method. A detailed process is as follows: an aqueous solution of $Cr(NO_3)_3$ was mixed with a $Y(OH)_3$ powder, then an aqueous solution of $(NH_4)_2CO_3$ (1 M) was added to the mixture under stirring until a precipitated slurry was obtained. The resulting slurry was aged for 2 h and then separated from the mother liquid, washed with deionized water and dried at 120 °C overnight. Finally, it was calcined at 400, 500, 600 and 800 °C for 4 h. The catalysts were denoted as CrYO-4, CrYO-5, CrYO-6 and CrYO-8, and the Cr content was 20 wt% in the catalyst.

2.2. Catalyst activation

Prior to use, the prepared catalyst was subject to a pre-fluorination process in order to activate the catalyst. The pre-fluorination was carried out in a stainless steel tubular reactor with a diameter of 1 cm and a length of 30 cm. 3 g of prepared CrYO catalyst was loaded into the reactor and dried at 260 °C for 2 h and at 350 °C for 2.5 h in N_2 at a flow of 30 ml min^{-1}. Then the N_2 flow was stopped and a mixture of HF (80 ml min^{-1}) and N_2 (20 ml min^{-1}) was introduced at 260 °C for 2 h and subsequently at 350 °C for 2.5 h. The CrYO-4, CrYO-5, CrYO-6 and CrYO-8 catalysts after the activation process were denoted as CrYF-4, CrYF-5, CrYF-6 and CrYF-8, respectively.

2.3. Fluorination reaction

The fluorination reactions were carried out in the same reactor after the catalyst activation, under atmospheric pressure. 3 g of the pre-fluorinated catalyst was loaded, corresponding to a catalyst volume of 3 ml. Flow rates of CF_3CH_2Cl and HF pre-heated at 30 °C were carefully controlled using mass flow controllers. The molar ratio of $HF/CF_3CH_2Cl = 10$ and the GHSV was 3000 h^{-1}. The gaseous products were analyzed by a gas chromatograph (Shimadzu GC-14C) equipped with a flame ionization detector (FID) and a HP GS-GASPRO capillary column.

2.4. Catalyst characterization

Surface areas of the catalysts were determined by the modified BET method from the N_2 sorption isotherms at 77 K on an Auto-sorb-1 apparatus. Scanning electron microscopy (SEM) images of the catalysts were obtained an a Hitachi S-4800 microscope equipped with an energy dispersion X-ray (EDX) attachment.

X-ray diffraction (XRD) patterns were collected on a Philips PW3040/60 powder diffractometer operating at 40 kV and 40 mA using Cu$K\alpha$ radiation in the 2θ range from 10 to 80° with a scan rate of 0.3° min^{-1}. The *in situ* XRD experiments were carried out using an Anton Paar TCU 750 chamber linked to the X-ray diffraction diffractometer, with a scan rate of 0.3° min^{-1} and the XRD patterns were recorded in air atmosphere. Phase composition and cell parameter were calculated by Rietveld [10] method using MID-JADE 6.5 software.

TG-DSC experiments of the catalysts were performed using a Netzsch STA 449C instrument. The experiments were carried out to a maximum temperature of about 800 °C with a heating rate of 10 °C min^{-1} in air (50 ml min^{-1}).

Raman spectra were obtained on a Renishaw RM1000 confocal microscope with exciting wavelength of 514.5 nm under ambient conditions, and the catalysts were hydrated. UV–visible diffuse reflectance spectra were recorded on a Thermo Evolution 500 spectrophotometer equipped with a labsphere RSA-UC-40. X-ray photonelectron spectroscopy (XPS) experiments were carried out on a VG ESCALAB MK2 system (Perkin–Elmer) with Al$K\alpha$ radiation ($h\nu = 1486.6$ eV). The pass energy was fixed at 20 eV to ensure sufficient sensitivity. Binding energies were calibrated by using the contaminant carbon (C 1s = 284.6 eV).

Reducibility of the catalysts was measured by means of H_2 temperature-programmed reduction (H_2-TPR) technique. 20 mg of the catalyst was placed in a quartz reactor, which was connected to a home made TPR apparatus. 5% H_2 in N_2 was introduced with a flow rate of 25 ml min^{-1}. The catalyst was heated from 150 to 800 °C at a heating rate of 20 °C min^{-1}. The amount of H_2 uptake during the reduction was measured using a thermal conductivity detector (TCD). Water produced during the reduction was trapped with a 5A molecular sieve.

Contents of Cr in the catalysts were determined by the inductively coupled plasma (ICP) technique.

3. Results

3.1. Structural characterization

Table 1 lists the surface areas of the CrYO and the CrYF catalysts. For the CrYO catalyst, the surface area first increased then decreased with further calcination temperature. For the CrYF catalyst, its surface area was much larger than the corresponding CrYO catalyst. Besides, as calcination temperature increased, the surface area declined dramatically. For example, the CrYF-4 catalyst calcined at 400 °C had a surface area

Table 1
BET surface areas of CrYO and CrYF catalysts

Calcination temperature (°C)	BET surface area (m^2 g^{-1})	
	CrYO catalysts	CrYF catalysts
400	7.9	60.7
500	19.1	46.1
600	16.6	25.3
800	12.3	11.6

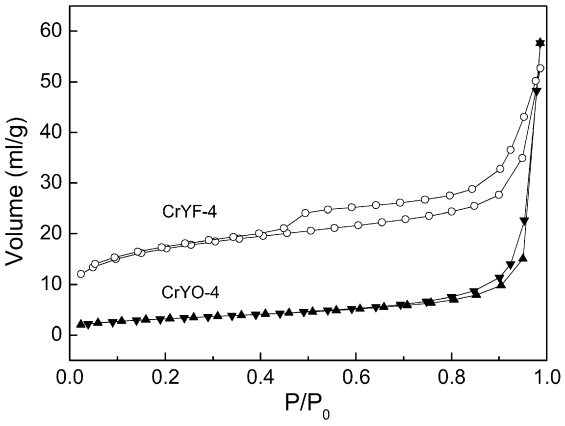

Fig. 1. N_2 sorption isotherms of CrYO-4 and CrYF-4 catalysts.

Table 2
Surface composition analysis of CrYO and CrYF catalysts by EDX

Calcination temperature (°C)	Atom (%)							
	CrYO catalyst				CrYF catalyst			
	Cr	Y	O	F	Cr	Y	O	F
400	14.1	41.0	44.9	/	12.2	45.1	0	42.7
500	9.4	50.7	39.9	/	8.6	47.0	2.1	42.3
600	13.7	53.6	32.7	/	14.8	36.7	10.2	38.3
800	16.8	54.1	29.1	/	16.1	56.0	27.9	0

of 60.7 $m^2\,g^{-1}$, while only 11.6 $m^2\,g^{-1}$ was obtained on the CrYF-8 catalyst calcined at 800 °C.

Fig. 1 shows the N_2 sorption isotherms of the CrYO-4 and the CrYF-4 catalysts. The N_2 sorption isotherms of the CrYF-4 catalyst was of type IV, indicating that it is a porous material. However, the isotherm of the CrYO-4 catalyst suggested that the catalyst is non-porous. Pore volumes of the CrYO-4 catalyst and the CrYF-4 catalyst are 0.089 ml g^{-1} and 0.076 ml g^{-1}, respectively. It should be noticed that the pore volume of the CrYO-4 catalyst is probably due to the particle packing effect. The microstructure of the representative catalyst calcined at 400 °C is shown in Fig. 2. It can be seen that the surface of CrYO-4 catalyst was very smooth while the CrYF-4 catalyst had some pore structure. Meanwhile, the surface composition analysis of the catalysts is listed in Table 2. For the CrYO catalysts, it was found that the oxygen concentration on the catalyst surface gradually decreased from CrYO-4 to CrYO-8. For the CrYF catalysts, oxygen concentration gradually increased while fluorine concentration gradually decreased with calcination temperature. It was interesting to find that the CrYF-8 catalyst had same surface composition as the CrYO-8 catalyst, indicating that the CrYO-8 catalyst could hardly be fluorinated during the activation process.

Fig. 3 shows the XRD patterns of the CrYO and the CrYF catalysts calcined at different temperatures. Phase compositions of the catalysts were summarized in Table 3. From Fig. 3a and Table 3, it can be seen that the CrYO-4 catalyst remained amorphous and the CrO_x species were well dispersed on the support surface. However, the characteristic peaks for $YCrO_4$ and Y_2O_3 were observed in the CrYO-5 and the CrYO-6 cata-

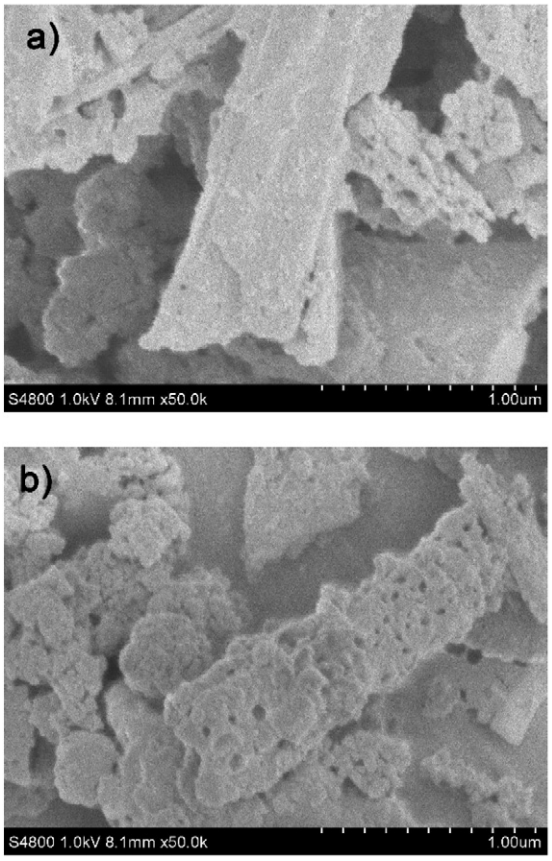

Fig. 2. SEM images for (a) CrYO-4 and (b) CrYF-4 catalysts.

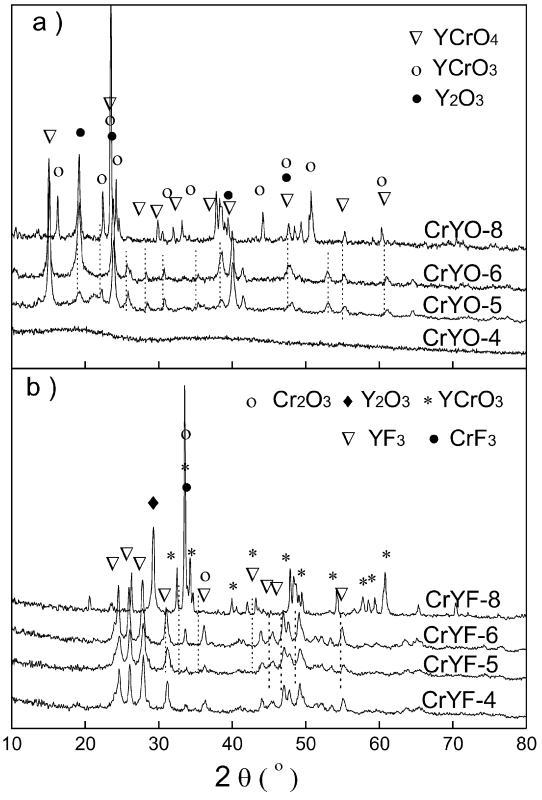

Fig. 3. XRD patterns of (a) CrYO and (b) CrYF catalysts.

Table 3
Phase and phase composition of CrYO and CrYF catalysts

Calcination temperature (°C)	Phase composition (wt%)	
	CrYO catalyst	CrYF catalyst
400	Amorphous	CrF_3 (6.8%) + YF_3 (93.2%)
500	$YCrO_4$ (67.2%) + Y_2O_3 (37.8%)	Cr_2O_3 (3.8%) + YF_3 (96.2%)
600	$YCrO_4$ (55.2%) + Y_2O_3 (44.8%)	Cr_2O_3 (18.6%) + YF_3 (81.4%)
800	$YCrO_3$ (68.8%) + Y_2O_3 (31.2%)	$YCrO_3$ (77.9%) + Y_2O_3 (22.1%)

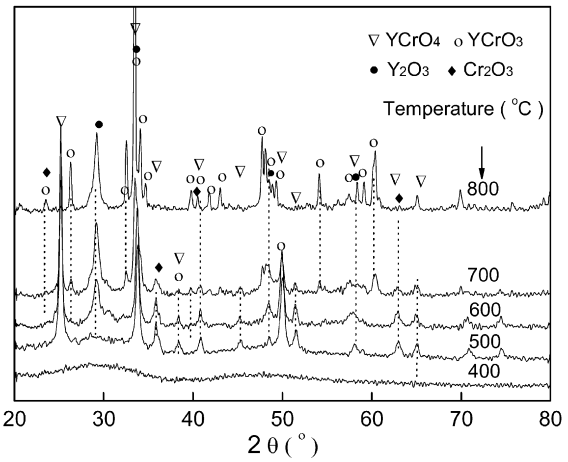

Fig. 4. *In situ* XRD patterns of CrYO-4 catalyst.

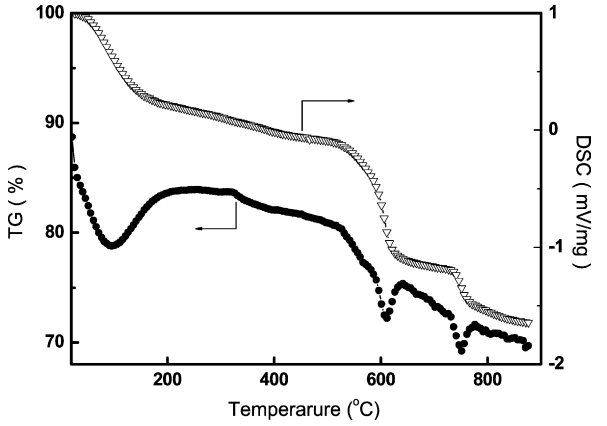

Fig. 5. TG/DSC curves of CrYO-4 catalyst.

Table 4
Phase and phase composition of CrYO-4 catalyst by *in situ* XRD results

Temperature (°C)	Phase composition (wt%)
400	Amorphous
500	$YCrO_4$
600	$YCrO_4$ (61.6%) + Y_2O_3 (38.4%)
700	$YCrO_4$ (35.1%) + $YCrO_3$ (26.8%) + Y_2O_3 (38.1%)
800	$YCrO_3$ (66.0%) + Y_2O_3 (34.0%)

Table 5
Raman shifts of the CrYO and CrYF catalysts

Calcination temperature (°C)	Raman shift (cm^{-1})	
	CrYO catalyst	CrYF catalyst
400	365, 890, 1100	209, 282, 343, 545, 698, 848, 1378
500	365, 545, 825, 865	209, 282, 343, 545, 698, 848, 1378
600	365, 545, 825, 870	209, 282, 343, 545, 698, 848, 1378
800	220, 280, 340, 490, 545, 698, 825, 1400	209, 217, 280, 340, 487, 545, 698, 848, 1378

lysts, and the intensity of Y_2O_3 peak increased with calcination temperature. When the catalyst was calcined at 800 °C, a new $YCrO_3$ phase appeared accompanied by the disappearance of the $YCrO_4$ phase.

As seen in Fig. 3b, for the CrYF-4 catalyst, characteristic peaks of CrF_3 and YF_3 were observed. Besides, crystalline YF_3 and Cr_2O_3 phases were detected in the CrYF-5 and the CrYF-6 catalysts, while the CrYF-8 catalyst had same structure as the CrYO-8 catalyst.

Fig. 4 presents *in situ* XRD patterns of the CrYO-4 catalyst, which clearly demonstrated the transformation of the CrO_x species during the heating process. The catalyst was amorphous at 400 °C, while the $YCrO_4$ phase emerged at 500–600 °C. With further increasing temperature, the $YCrO_3$ and Cr_2O_3 phases appeared. This result is in good agreement with the XRD results obtained from the catalysts calcined at different temperatures, indicating the CrO_x species transformed from high oxidation state (Cr(VI)) to low oxidation state (Cr(III)). Furthermore, phase composition analysis summarized in Table 4 shows that the CrO_x species composition is in good accordance with that in Table 3.

The TG/DSC experiments were conducted to further illustrate the transformation of CrO_x species for the CrYO-4 catalyst during the calcination process and the results are shown in Fig. 5. As seen in Fig. 5, an obvious weight loss was observed below 200 °C, which could be attributed to the loss of crystalline H_2O. In addition, a main weight loss was observed between 500 and 650 °C, accompanied by a strong endothermic peak at 610 °C. Also, a weight loss at about 750 °C was observed with an endothermic peak.

The Raman spectra of CrYO and CrYF catalysts with different calcination temperatures are shown in Fig. 6 and the Raman shifts are summarized in Table 5. Note that no Raman band at 376 cm^{-1} assigned to Y_2O_3 was observed for all the catalysts. For the CrYO-4 catalyst, two Raman peaks were observed at 365 and 890 cm^{-1}, which were assigned to the symmetric stretching and bending modes of Cr(VI), respectively, corresponding to isolated tetrahedral surface-chromate species that was distorted by its interaction with the oxide support surface [4,11–13]. For the CrYO-5 and the CrYO-6 catalysts, they show a strong band at 865 cm^{-1} and a shoulder band at 825 cm^{-1} due to oligomeric (dimer to tetramer) species of CrO_x [4,14]. Additionally, a Raman band at 545 cm^{-1} indicated the presence

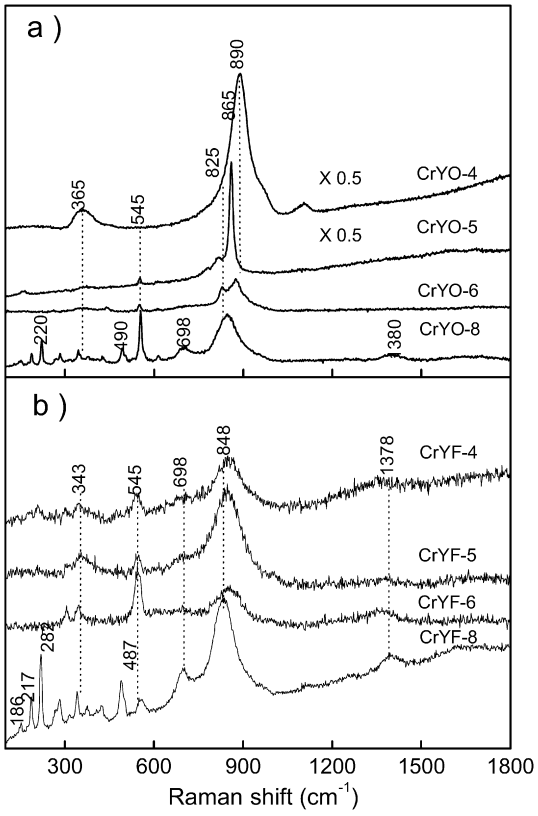

Fig. 6. Raman spectra of (a) CrYO and (b) CrYF catalysts.

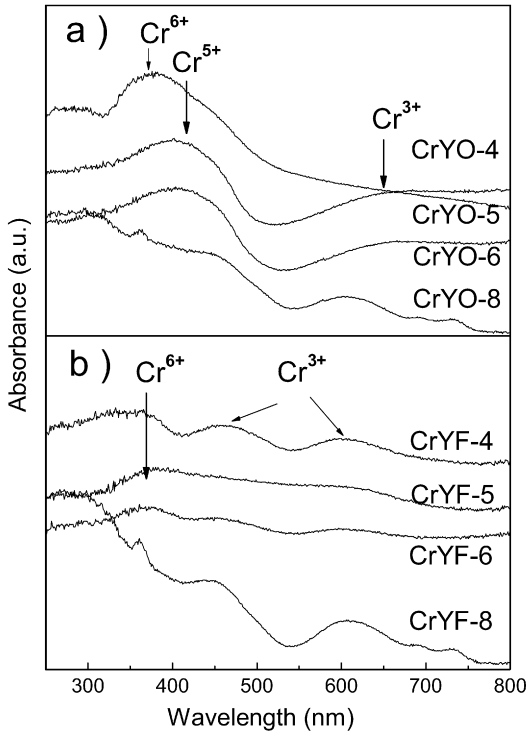

Fig. 7. UV–vis diffuse reflectance spectra of (a) CrYO and (b) CrYF catalysts.

of crystalline Cr_2O_3 [11,15,16], while the band at 365 cm^{-1} almost disappeared. For the CrYO-8 catalyst, in addition to a band at 825 cm^{-1} due to oligomeric species of CrO_x, a new band at 220 cm^{-1} due to the Cr–O–Cr band vibration of dichromate was observed [11,17]. The bands at 489, 545, 698 and 1380 cm^{-1} were assigned to the crystalline Cr_2O_3. The weak peak intensity for the CrYO-6 catalyst was due to the dark green color of the catalyst. The shift of the main Raman band (800–900 cm^{-1}) towards lower frequency indicated that the degree of polymerization of the CrO_x species in the catalyst increased with calcination temperature [4,14].

Fig. 6b shows the Raman spectra of the CrYF catalysts. It should be noted that YF_3 gave no Raman signal under the ambient conditions. For all the catalysts, the bands at about 343 and 848 cm^{-1} due to the Cr–O stretching and bending modes of the Cr(VI) oxides were observed. Besides, the bands assigned to Cr–O–Cr linkages (220 cm^{-1}) and crystalline Cr_2O_3 (548 cm^{-1}) were also observed. All the catalysts show a band at 1378 cm^{-1} assigned to the crystalline Cr_2O_3, which was probably formed during the fluorination process. For the CrYF-8 catalyst, no obvious change was found compared to the CrYO-8 catalyst.

In order to further illuminate the oxidation state of Cr species in the CrYO and CrYF catalysts, the UV–visible diffuse reflectance experiments were carried out and the results are shown in Fig. 7. In Fig. 7a, a broad absorption peak at about 370 nm assigned to Cr(VI) [18–20] was detected for the CrYO-4 catalyst, indicating that the surface CrO_3 species in Cr(VI) oxidation state were predominant at 400 °C. But the CrYO-5 and the CrYO-6 catalysts show two absorption peaks at 410 and 600–700 nm, which were assigned to the Cr^{5+} and Cr^{3+}, respectively [16,17]. When the calcination temperature increased to 800 °C, the peak intensity at 370 nm corresponding to Cr^{6+} dramatically decreased, while peaks at 475 nm and 600–730 nm appeared, suggesting that the oxidation state changed from Cr(VI) to Cr(III) at high calcination temperature.

In Fig. 7b, all the CrYF catalysts show a band at 370 nm, indicating some Cr^{6+} species still existed. However, for the CrYF-4 catalyst, two new bands at 465 and 610 nm due to Cr^{3+} appeared. For the CrYF-5 and CrYF-6 catalysts, the intensity of these two bands was slightly weaker. Like the XRD and Raman results, the UV–visible diffuse spectra of CrYF-8 catalyst remained the same as the CrYO-8 catalyst.

XPS experiments were conducted to further investigate the CrO_x species on the catalysts surface. Fig. 8 shows the Cr 2p XPS spectra of the CrYO and the CrYF-4 catalysts. For the CrYO-4 catalyst, the Cr $2p_{3/2}$ peak was resolved into two peaks at 579.4 and 576.8 eV. The former peak was assigned to the CrO_3 and the latter one was assigned to the amorphous Cr_2O_3 phase [8,21–23]. For the CrYO-5 catalyst, the Cr $2p_{3/2}$ core level shows two peaks at 578.5 and 576.3 eV, which were assigned to the $YCrO_4$ phase and the Cr_2O_3 phase, respectively. For the CrYO-6 catalyst, the peaks at 578.5 and 577.3 eV were ascribed to the $YCrO_4$ and $YCrO_3$ phases, respectively. For the CrYO-8 catalyst, the peak at 578.7 eV was assigned to the $YCrO_3$ phase and the peak at 575.8 eV indicated the presence of Cr_2O_3. The shift of the main peak at 579.4 eV to lower binding energy suggested the transformation of high oxidation state

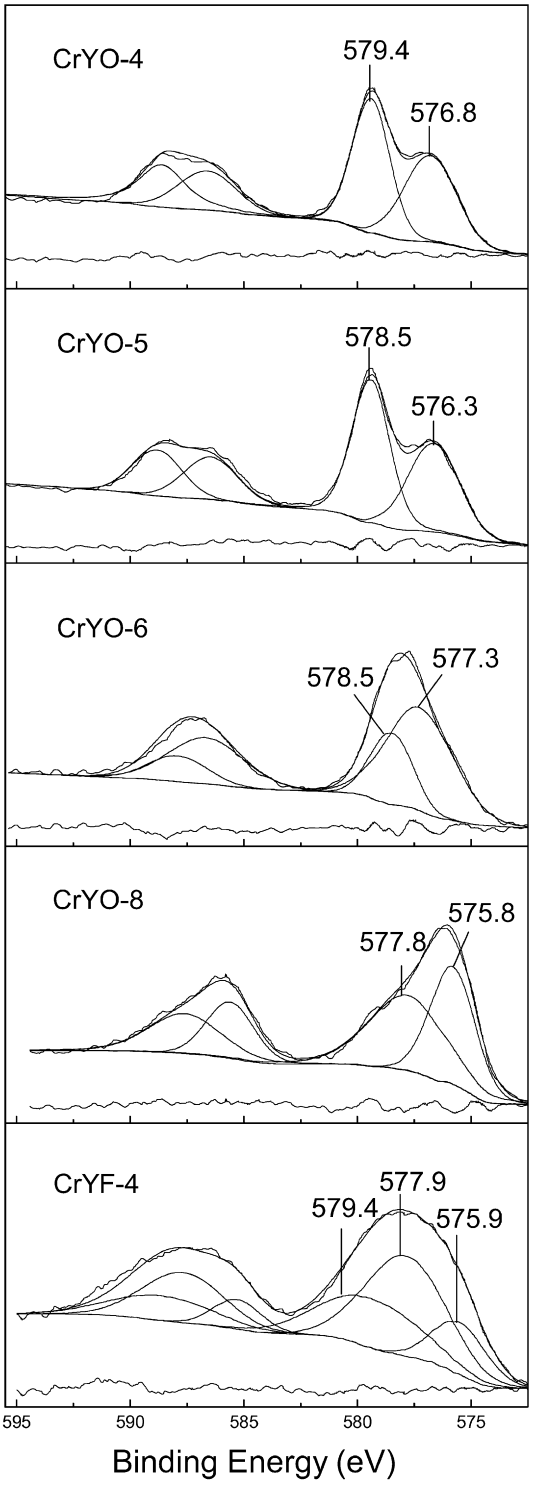

Fig. 8. XPS spectra of Cr 2p for the CrYO and CrYO-4 catalysts.

Table 6
Amount of Cr species with different valences on catalysts by XPS analysis

Catalyst	Cr content (%)
CrYO-4	Cr^{6+} (53.5%) + Cr^{3+} (46.5%)
CrYO-5	Cr^{5+} (68.6%) + Cr^{3+} (31.4%)
CrYO-6	Cr^{5+} (29.8%) + Cr^{3+} (71.2%)
CrYO-8	Cr^{3+} (100.0%)

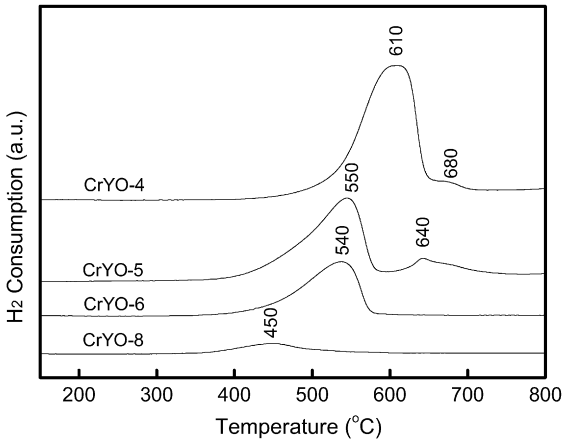

Fig. 9. TPR profiles of CrYO catalysts.

Table 7
Total amounts of H_2 consumption values obtained from TPR profiles

Catalyst	H_2 consumption (mmol g_{cat}^{-1})
CrYO-4	3.3
CrYO-5	2.6
CrYO-6	1.4
CrYO-8	0.3

Cr(VI) species to low oxidation state Cr(III) species during the calcination process.

The contents of Cr species with different valences in the CrYO catalysts were listed in Table 6, derived from the peak area of the corresponding Cr species from the XPS results. For the CrYO-4 catalyst, the contents of Cr^{6+} and Cr^{3+} species were 53.5 and 46.5%, respectively. For the CrYO-5 and the CrYO-6 catalysts, the content of Cr^{5+} species decreased while the content of Cr^{3+} species increased with calcination temperature. For the CrYO-8 catalyst, the content of Cr^{3+} species ($YCrO_3 + Cr_2O_3$) was 100%.

The Cr 2p XPS spectrum of the CrYF-4 catalyst was also recorded in Fig. 8. For the CrYF-4 catalyst, the Cr $2p_{3/2}$ core level shows three peaks at 579.4, 577.9 and 575.9 eV. The peak at 579.4 eV was assigned to CrF_3, and the peak at 577.9 eV may be attributed to the formation of $Cr(OH)_xF_y$ by fluorination of CrO_x [24], and peak at 575.9 eV was assigned to Cr_2O_3 phase. It should be noticed that EDX results of the CrYF-4 catalyst (Table 2) did not reveal the existence of oxygen; however, it is probably due to the detection limit of the apparatus (0.5 at%).

The H_2-TPR profiles of the CrYO catalysts are shown in Fig. 9. The total amounts of H_2 consumption are listed in Table 7. The CrYO-4 catalyst shows one reduction peak centered at 610 °C and one weak reduction peak at 680 °C. The former was related to the more easily reducible oligomeric chromate while the latter to the less reducible monochromate [14]. The reduction peaks shifted to the lower temperature at 550 and 640 °C when the calcination temperature increased to 500 °C. Moreover, these two peaks incorporated into one when calcination temperature increased to 600 and 800 °C, and the peak position shifted to a lower temperature. For the CrYO-8 catalyst, only a reduction weak peak at 450 °C was observed.

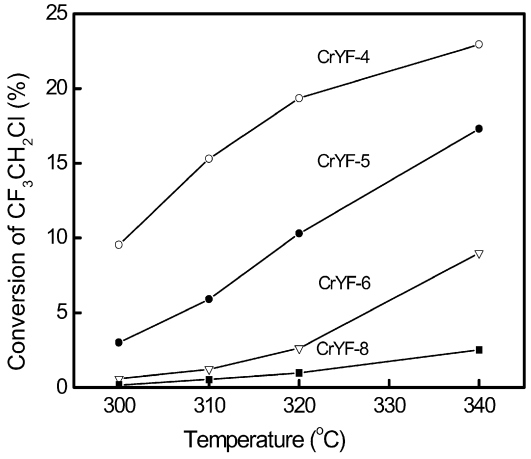

Fig. 10. Fluorination of CF_3CH_2Cl over various CrYF catalysts. Reaction conditions: $HF/CF_3CH_2Cl = 10$, S.V. $= 3000\ h^{-1}$.

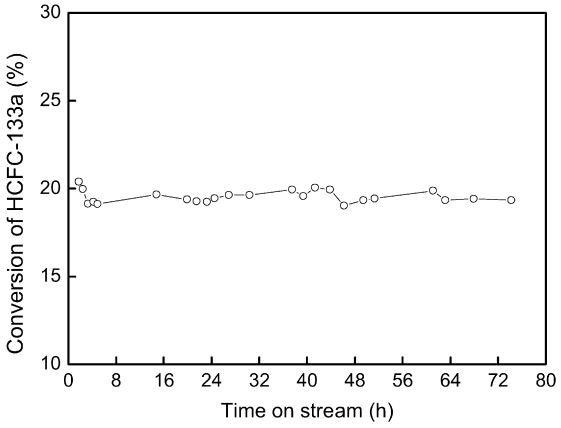

Fig. 11. Fluorination of CF_3CH_2Cl over CrYF-4 catalyst with time on stream at 320 °C. Reaction conditions: $HF/CF_3CH_2Cl = 10$, S.V. $= 3000\ h^{-1}$.

As seen in Table 7, H_2 consumption amount varies from 3.3 to 0.3 mmol $H_2\ g_{cat}^{-1}$ as the calcination temperature increased from 400 to 800 °C.

3.2. Catalytic testing

Fig. 10 shows the effect of calcination temperature on the catalytic performance of the CrYF catalysts. Note that the selectivity to CF_3CH_2F was not given for it was higher that 98%. It can be seen that calcination temperature has great influence on the catalytic activity. The catalyst calcined at low temperature had higher activity than the one calcined at high temperature. For example, about 19% of CF_3CH_2Cl conversion was obtained on the CrYF-4 catalyst at 320 °C, while less than 5% of conversion was obtained on the CrYF-8 catalyst.

Fig. 11 demonstrates stability of the pre-fluorinated CrYO-4 catalyst (CrYF-4) at 320 °C under reaction conditions. It could be seen that the conversion slightly decreased in the initial period and it reached steady state after 3 h.

In order to investigate the change of the catalyst structure after different reaction time, Fig. 12 shows XRD patterns of the

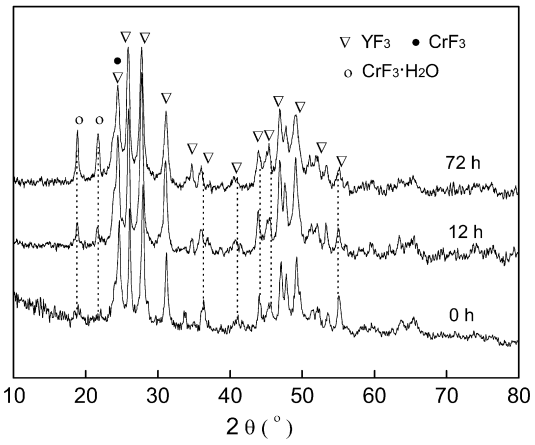

Fig. 12. XRD patterns of CrYF-4 catalyst after different reaction time.

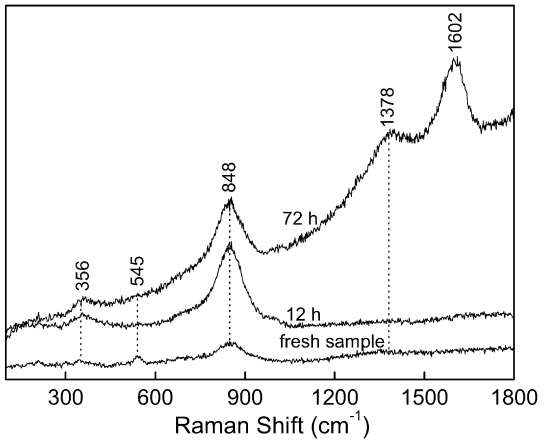

Fig. 13. Raman spectra of CrYF-4 catalyst after different reaction time.

CrYF-4 catalyst after different reaction time. $CrF_3{\cdot}H_2O$ phase was observed in the CrYF-4 catalyst after 12 h reaction, and the peak intensity increased with further 72 h reaction. Also, Raman spectra of the CrYF-4 catalyst after different reaction time is shown in Fig. 13. With increasing reaction time, the peak intensity of CrO_x became stronger, and a new band at 1602 cm^{-1} due to carbon was observed [25].

4. Discussion

4.1. Effect of calcination temperature on the catalyst structure

In this work, a series of CrYO catalysts were prepared and the effect of calcination temperature on the CrO_x species was investigated. For the CrYO catalysts, relatively low surface areas were obtained, while the pre-fluorinated catalysts (CrYF) have much higher surface area than the CrYO catalysts except the CrYF-8 catalyst (Table 1). The pre-fluorination process probably caused a change in catalyst structure because of the reaction between HF and the CrYO catalyst, as evidenced by the N_2 sorption isotherms (Fig. 1) and the SEM results (Fig. 2). The porous CrYF-4 catalyst results in a higher surface area compared to the CrYO-4 catalyst. Additionally, by compar-

ing the images of the CrYO-4 and the CrYF-4 catalysts, the more porous morphology of the CrYF-4 catalyst suggests that it could be responsible for the increase in surface area after pre-fluorination.

The XRD (Figs. 3 and 4) and the Raman (Fig. 6) results reveal the general phase transformation of the chromium species. In the CrYO-4 catalyst, the chromium oxide are well dispersed on the support and mainly exist in the form of high oxidation state Cr(VI). With increasing calcination temperature, phases of $YCrO_4$ and $YCrO_3$ with support Y_2O_3 were observed. The interaction between CrO_3 and Y_2O_3 at low and high temperature may follow the equations [26]:

$$2CrO_3 + Y_2O_3 \rightarrow 2YCrO_4 + (1/2)O_2, \quad (1)$$

$$YCrO_4 \rightarrow YCrO_3 + (1/2)O_2. \quad (2)$$

As seen from the Raman spectra (Fig. 6a), CrO_x species in the CrYO-4 catalyst was probably in form of CrO_3. The isoelectric point (IEP) of Y_2O_3 is 8.1, which is close to that of Al_2O_3 (8.9). Previous research pointed out that the chromium species on the Al_2O_3 contains chromate and dichromate [12], which is consistent with the current study, as evidenced by the H_2-TPR results (Fig. 9). As the calcination temperature increased from 500 to 800 °C, the crystalline Cr_2O_3 was observed and the isolated CrO_x species transformed to the oligomeric (dimer to tetramer) species. For the CrYO-8 catalyst, the intensity of the crystalline Cr_2O_3 Raman band further increases, which indicates a larger proportion of Cr_2O_3 in the catalyst. Additionally, in the Raman spectra, the band due to Y_2O_3 (376 cm^{-1}) was not observed probably due to the fact that the CrO_x species aggregates on the catalyst surface and cover the Y_2O_3 support, particularly at high Cr loading (20%). UV–vis (Fig. 7) and XPS (Fig. 8) results clearly identified the different Cr species in the CrYO and the CrYF catalysts, which again confirmed the different Cr species in the catalysts. The existence of the bands at 465 and 610 nm in the CrYF-4 catalysts suggested the emergence of Cr^{3+} species during the fluorination process.

TG/DSC result (Fig. 5) indicated that two endothermic peaks between 600 and 800 °C were observed. The peak at 610 °C is probably assigned to the transformation of Cr species from the high oxidation state Cr(VI) to the low oxidation state Cr(V), and the peak below 800 °C is due to the transformation from Cr(V) to the lower oxidation state Cr(III) [26]. This is consistent with the *in situ* XRD result.

The binding energy values of Cr $2p_{3/2}$ in the CrYO catalysts (Fig. 8) shift to lower values with increasing calcination temperature, indicating the average oxidation state of CrO_x becomes lower. These results are in line with the XRD, Raman and UV–vis results.

H_2-TPR results (Fig. 9) shows a clear shift of the reduction peaks. The shift is probably related to interaction between the CrO_x species and the support. For the catalysts calcined at low temperature, the interaction of CrO_x species with the support is very strong, which makes the reduction of the CrO_x species difficult. While for the catalysts calcined at high temperature, the interaction between the CrO_x species and the support becomes weaker because of the growth of the crystalline size of CrO_x species, therefore the reduction of the CrO_x species becomes easier. In other hand, as reported previously, the reduction of polymeric chromate is easier than the monochromate [14], high calcination temperature makes a higher degree of polymerization of CrO_x species, as evidenced by Raman results (Fig. 6a), which results in a lower reduction temperature.

H_2 consumption amounts of the CrYO catalysts decrease with increasing calcination temperature (Table 7). Note that the reduction of CrO_3 may follow two steps:

$$CrO_3 + (3/2)H_2 \rightarrow (1/2)Cr_2O_3 + (3/2)H_2O, \quad (3)$$

$$Cr_2O_3 + (3/2)H_2 \rightarrow (1/2)Cr + (3/2)H_2O. \quad (4)$$

However, the reduction of Cr_2O_3 to Cr (Eq. (2)) is not likely to occur below 800 °C [27,28]. Also, the consumption values are much lower than the stoichiometric value of H_2 consumption (5.8 mmol g_{cat}^{-1}), if one assumes that all the Cr(VI) species could be reduced to Cr(III), especially for the catalysts calcined at high temperature. Note that the XRD, Raman and UV–vis results (Figs. 3a, 6a and 7a) clearly show that the high oxidation state Cr content decreases with calcination temperature. Therefore, the reduction peaks found in the present work is likely due to the reduction of fractional high oxidation state Cr(VI) or Cr(V) on the catalyst surface to Cr(III), as the XRD results (Fig. 3a) and the Raman results (Fig. 6a) clearly show the existence of Cr(VI) and Cr(V) species.

4.2. Active sites for the fluorination reaction

Since the pre-fluorination process is necessary in order to activate the catalyst, it is more important to investigate the CrYF catalysts because it may provide relevant information of the active sites for the fluorination reaction.

The phase composition of the CrYF catalysts was also confirmed by the XRD (Fig. 3b) and the Raman (Fig. 6b) results. It was found that the high oxidation state Cr species (Cr(VI)) transformed to low oxidation state Cr species (Cr(III)). Also, in the CrYF-4, CrYF-5 and CrYF-6 catalysts, the support Y_2O_3 transformed to YF_3. Moreover, comparing to the CrYF-8 catalyst with the CrYO-8 catalyst, XRD results (Fig. 3) found that the features merely changed, indicating that the CrYO-8 catalyst is very stable during the fluorination process. Raman results (Fig. 6b) indicated that the CrO_x species become polymeric during the fluorination process, and the polymeric chromates are difficult to be fluorinated [4]. EDX composition analysis (Table 2) shows that the F concentration in the CrYF catalysts decreased with calcination temperature. Note that the CrYO-4 catalyst contains isolated Cr(VI) species while the CrYO-8 catalyst contains oligomeric Cr(VI) and dominant Cr(III) species. XPS results (Fig. 8) on the CrYF-4 catalyst reveal the existence of CrF_3, $Cr(OH)_xF_y$ and Cr_2O_3 species, so it could be concluded that the evolution of these species was originated from the well isolated high oxidation state Cr(VI) on the catalyst surface, whereas the low oxidation state chromium compounds $YCrO_3$ and Cr_2O_3 or the Cr(VI) species in oligomeric form

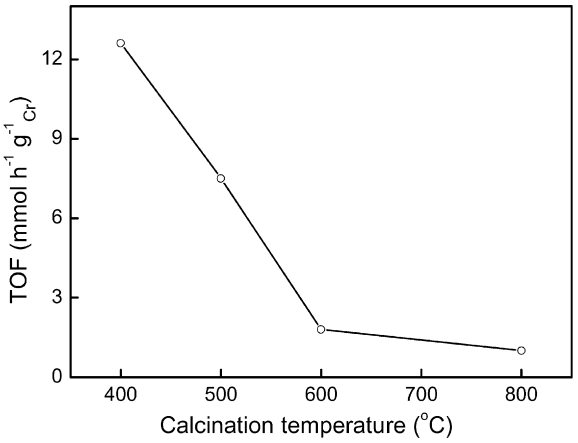

Fig. 14. Turnover frequency (TOF) for fluorination of CF_3CH_2Cl over CrYO catalysts calcined at different temperatures (calculated based on the total Cr content in the catalyst, reaction temperature 320 °C).

is difficult to be fluorinated by HF. Furthermore, UV–vis results (Fig. 7b) confirmed the transformation of Cr species. In the CrYF-4, the appearance of Cr(III) species indicates that partial Cr(VI) was reduced during the pre-fluorination process, and the higher intensity of the Cr(III) in the CrYF-4 catalyst than in other catalysts suggests that higher proportion of Cr(VI) species in the CrYO-4 catalyst was transformed.

The prepared CrYO-4 catalyst has higher reactivity compared to the best catalyst that had been reported. Cho et al. [4] prepared a Cr/MgO catalyst and found that the catalytic activity was greatly affected by the support and activating conditions. The highest conversion obtained on the Cr/MgO catalyst was about 10% at 320 °C ($HF/CF_3CH_2Cl = 8$, $GHSV = 1800\ h^{-1}$). In another group, Lee et al. [6] prepared a Cr/MgF_2 catalyst and the best initial catalytic activity was $0.68\ mmol\,h^{-1}\,g_{cat}^{-1}$ at 320 °C ($HF/CF_3CH_2Cl = 8$). In our study, the highest conversion obtained on the CrYO-4 was about 19% at 320 °C ($HF/CF_3CH_2Cl = 10$, $GHSV = 3000\ h^{-1}$), corresponding to a formation rate of $2.03\ mmol\,h^{-1}\,g_{cat}^{-1}$. Besides, the catalyst is stable even after 72 h reaction time. This indicates that the Cr catalysts supported on Y_2O_3 could be a promising candidate for the fluorination reaction.

Turnover frequency (TOF) of the reaction calculated based on the total Cr content in the catalyst is shown in Fig. 14. It was found that the TOF decreased with increasing calcination temperature. As the total amount of Cr in the catalysts is nearly the same, however, the amount of the CrO_x species with high oxidation state (>Cr(III)) decreased from CrYO-4 to CrYO-8. Cho et al. [4] and Adamczyk et al. [7] concluded that chromium fluoride CrF_x or oxyfluoride CrO_xF_y species are the active sites for the fluorination of CF_3CH_2Cl to CF_3CH_2F. Our finding supports their conclusion because the activity closely correlates with the pre-fluorinated Cr species. Furthermore, the new finding in this study is that the origin of the fluorinated Cr species was identified, that is, the well isolated Cr(VI) species on the catalyst surface could be transformed to CrF_x, CrF_xO_y or $Cr(OH)_xF_y$ species.

5. Conclusions

A series of CrO_x–Y_2O_3 catalysts with different calcination temperatures have been prepared for vapor-phase fluorination of CF_3CH_2Cl to synthesize CF_3CH_2F. The highest activity was obtained on a pre-fluorinated catalyst calcined at 400 °C, with 19% of CF_3CH_2Cl conversion at 320 °C. The calcination temperature of the catalyst has great influence on the CrO_x species. With increasing calcination temperature, the structure of the CrO_x species transformed from the highly dispersed monochromate (CrO_3) to low oxidation state CrO_x species (Cr(V) and Cr(III)) and oligomeric chromate. During the activation process, partial well dispersed monochromate (CrO_3) transformed to the catalytically active species CrF_x, CrO_xF_y or $Cr(OH)_xF_y$. As the content of the well dispersed monochromate decreased with increasing calcination temperature, it led to a decline in activity.

Acknowledgments

This work is financially supported by the Zhejiang Provincial Nature Science Foundation of China (Grant No. Y407179). We also thank Prof. Wei-xin Huang (University of Science and Technology of China) for XPS peak fitting.

References

[1] M.L. Molina, F.S. Rowland, Nature 249 (1974) 810.
[2] S. Brunet, B. Requieme, E. Colnay, J. Barrault, M. Blanchard, Appl. Catal. B 5 (1995) 305.
[3] S. Brunet, B. Requieme, E. Matouba, J. Barrault, M. Blanchard, J. Catal. 152 (1995) 70.
[4] D.H. Cho, Y.G. Kim, M.J. Chung, J.S. Chung, Appl. Catal. B 18 (1998) 251.
[5] H. Lee, H.S. Kim, H. Kim, W.S. Jeong, I. Seo, J. Mol. Catal. A 136 (1998) 85.
[6] H. Lee, H.D. Jeong, Y.S. Chung, H.G. Lee, M.J. Chung, S. Kim, H.S. Kim, J. Catal. 169 (1997) 307.
[7] B. Adamczyk, O. Boese, N. Weiher, S.L.M. Schroeder, E. Kemnitz, J. Fluorine Chem. 101 (2000) 239.
[8] Y.S. Chung, H. Lee, H.D. Jeong, Y.K. Kim, H.G. Lee, H.S. Kim, S. Kim, J. Catal. 175 (1998) 220.
[9] H.D. Quan, M. Tamura, Y. Matsukawa, J. Mizukado, T. Abe, A. Sekiya, J. Mol. Catal. A 219 (2004) 79.
[10] R.A. Young, The Rietveld Method, Oxford Univ. Press, Oxford, 1993, p. 22.
[11] B.M. Weckhuysen, I.E. Wachs, J. Chem. Soc. Faraday Trans. 92 (1996) 1969.
[12] B.M. Weckhuysen, I.E. Wachs, R.A. Schoonheydt, Chem. Rev. 96 (1996) 3327.
[13] B.M. Weckhuysen, R.A. Schoonheydt, J.M. Jehng, I.E. Wachs, S.J. Cho, R. Ryoo, S. Kijlstra, E. Poels, J. Chem. Soc. Faraday Trans. 91 (1995) 3245.
[14] S.D. Yim, I.S. Nam, J. Catal. 221 (2004) 601.
[15] M. Cherian, M.S. Rao, A.M. Hirt, I.E. Wachs, G. Deo, J. Catal. 211 (2002) 482.
[16] O.F. Gorriz, L.E. Cadús, Appl. Catal. A 180 (1999) 247.
[17] F.D. Hardcastle, I.E. Wachs, J. Mol. Catal. 46 (1988) 173.
[18] B. Sun, E.P. Reddy, P.G. Smirniotis, Appl. Catal. B 57 (2005) 139.
[19] R. Galindo, J.A. Badenes, M. Llusar, M.A. Tena, G. Monrós, Mater. Res. Bull. 42 (2007) 437.

[20] M. Cherian, M.S. Rao, W.T. Yang, J.M. Jehng, A.M. Hirt, G. Deo, Appl. Catal. A 233 (2002) 21.

[21] D. Chidambaram, G.P. Halada, C.R. Clayton, Appl. Surf. Sci. 181 (2001) 283.

[22] E. Kemnitz, A. Kohne, I. Grohmann, A. Lippitz, W.E.S. Unger, J. Catal. 159 (1996) 270.

[23] P.G. Harrison, N.C. Lloyd, W. Daniell, J. Phys. Chem. B 102 (1998) 10672.

[24] J.M. Rao, A. Sivaprasad, P.S. Rao, B. Narsaiah, S.N. Reddy, V. Vijayakumar, S.V. Manorama, K.L. Krishna, K. Srinivas, K.R. Krishman, S. Badrinarayanan, J. Catal. 184 (1999) 105.

[25] R. Escribano, J.J. Sloan, N. Siddique, N. Sze, T. Dudev, Vib. Spectrosc. 26 (2001) 179.

[26] T. Tachiwaki, Y. Kunifusa, M. Yoshinaka, K. Hirota, O. Yamaguchi, Int. J. Inorg. Mater. 3 (2001) 107.

[27] X. Wang, Y.C. Xie, Appl. Catal. B 35 (2001) 85.

[28] X. Wang, Y.C. Xie, Catal. Lett. 75 (2001) 73.